MIMO Subband Volterra Digital Predistortion for Concurrent Aggregated Carrier Communications

Efrain Zenteno, *Member, IEEE*, and Daniel Rönnow, *Member, IEEE*

***Abstract*— This paper presents a multiple-input multiple-output (MIMO) nonlinear mitigation technique for closely spaced concurrent aggregated carrier systems. The transmitter architecture considers band-limited sources, where the predistorter and signal bandwidth are the same, thus reducing transmitter hardware cost and power consumption. The technique relies on multirate processing and linear filtering and uses the carrier frequencies to isolate the contribution of linear and nonlinear basis functions to the desired bands. This approach can be used with any MIMO model structure. In particular, models are linear in the parameters of low computational complexity. The technique was evaluated using three concurrent carriers of 50 MHz each fed to a Doherty amplifier. The results show significant reduction in the error vector magnitude and improvements for the transmitter efficiency using the proposed compensation technique.**

***Index Terms*— Concurrent, digital predistortion (DPD), memory polynomials, MIMO, multiband, multiple-input multiple-output (MIMO) predistortion, power amplifier linearization, power amplifiers, Volterra.**

I. Introduction

THE increasing need of capacity in wireless communications is leading to the deployment of multiple signals in the radio frequency (RF) front end. For such deployments, two distinct technologies are being considered. First, multiple-input multiple-output (MIMO) transmitters; or so-called, multiple antenna transmitters [1] with its corresponding compensation techniques [2]. Second, concurrent carrier systems are also a candidate technology [3]. That is, frequency-multiplexed multiple-RF transmissions or multiband transmissions. This paper deals with the latter.

Multiband transmission systems can be deployed using different hardware (HW) architectures. Considering the reuse of HW and its power efficiency, the concurrent transmitter architecture is favored over other possible candidates [3]. In a concurrent carrier architecture, the input is a frequency-multiplexed (enlarged bandwidth) signal forwarded through a power amplifier. Concurrent transmissions are considered in terrestrial communications, such as the long-term evolution standard [4], and in satellite systems where several carriers are frequency-multiplexed sharing the on-board satellite resources [5]. Operating concurrent amplifiers at high power efficiency produces significant levels of distortion that deteriorates the link quality [6]. This is the background for numerous compensation techniques, among which digital predistortion (DPD) is one of the most extensively used [7].

In concurrent amplification, the nonlinear distortions appear at frequency lines, which are linear combinations of the input frequencies. While the traditional single-carrier single-input single-output (SISO) DPD schemes require large bandwidth with increased costs [8], MIMO DPD of concurrent transmitters considers independent baseband processing per carrier requiring narrower individual bandwidth; therefore, MIMO DPD reduces HW costs and processing requirements [9].

The MIMO Volterra theory [10], [11] presents a solid theoretical framework for developing MIMO DPD model structures. However, the MIMO Volterra series exhibits increased complexity that motivates its pruning for application deployment. Pruning can be made based on several approaches, i.e., signal processing [12], bandwidth effects [13], and sparse sensing [14]. The MIMO Volterra series can be considered a general form of the memory polynomial model. Among the polynomial models, orthogonal memory polynomials offer improved numerical robustness and were implemented in a field programmable gate array in [15]. Besides polynomial models, concurrent transmitters have been modeled and predistorted using neural networks [16], lookup tables [17], distortion-canceling injection methods [18], rational polynomial functions [19], and spline interpolations [15], [20]. The mentioned studies, which are for concurrent systems, consider the case of the carriers being largely frequency spaced, so that, nonlinear products are frequency distant and hence isolated from each other.

Bassam *et al.* [21] rely on undersampling and in frequency-distant dual carriers, with a careful choice of sampling frequency, the aliasing effect created a measurement of the two carriers not interfering within each other. In this paper, we consider closely spaced carriers generated from multiple source generators as foreseen in power-efficient architectures in carrier aggregated systems [3].

In this paper, the power amplifier is cascaded by a bandpass filter removing distortions out of the frequency-multiplexed band. Although a filter at the transmitter output is undesirable

Manuscript received January 22, 2016; revised June 15, 2016, August 10, 2016, and November 10, 2016; accepted November 12, 2016. Date of publication January 9, 2017; date of current version March 3, 2017.

E. Zenteno was with the Department of Electronics, Mathematics, and Natural Sciences, University of Gävle, SE 80176 Gävle, Sweden, and also with the Department of Signal Processing, Royal Institute of Technology KTH, SE-100 44 Stockholm, Sweden. He is now with the Electronics and Telecommunication Department, Universidad Catolica San Pablo, Arequipa PE 04000, Peru (e-mail: ezenteno@ucsp.edu.pe).

D. Rönnow is with the Department of Electronics, Mathematics, and Natural Sciences, University of Gävle, SE 80176 Gävle, Sweden (e-mail: daniel.ronnow@hig.se).

Color versions of one or more of the figures in this paper are available online at http://ieeexplore.ieee.org.

Digital Object Identifier 10.1109/TMTT.2016.2630066

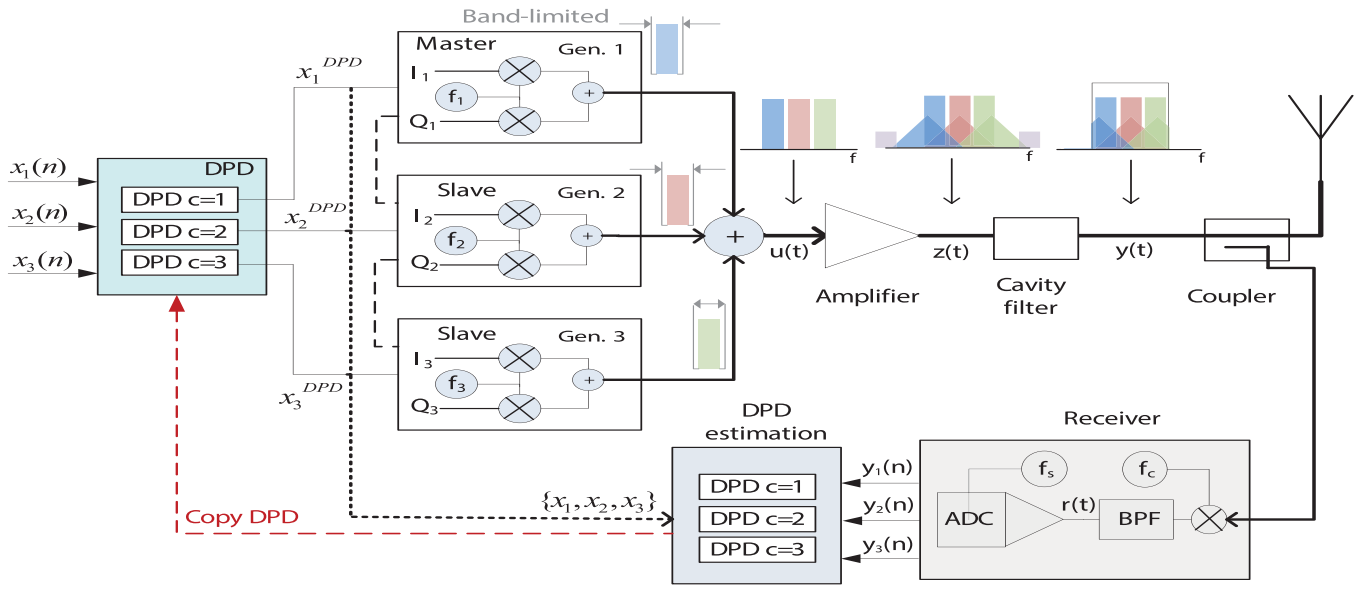

Fig. 1. Concurrent triband transmitter with feedback loop for digital predistortion. Each generator is band limited to the excitation signal. A bandpass filter removes unwanted out-of-band distortions.

from cost and size perspectives, the aid of such a filter has appeared in contemporary RF systems in multiple contexts: 1) to reduce the data rate processing in compensation techniques in SISO [22] and concurrent transmitters [23]; 2) to reduce the bandwidth in the instrumentation (feedback measurements) avoiding expensive ADCs [8]; and 3) to avoid spectrum regrowth of the DPD signal given a constrained uplink (in remote DPD systems) [24]. Furthermore, in this paper, the analog bandwidth of each generator is constrained to the signal bandwidth per channel. That is, each signal is sampled at its Nyquist rate that is the same rate of the DAC in the generator. Hence, this reduces the cost of the DAC stage and its power consumption as noted by Walden's metric [25]. Although, Walden's metric describes the metrics of performance/energy consumption for ADCs, it applies in the same way to DACs. This transmitter architecture is shown in Fig. 1.

The transmitter considered in this paper aggregates K carrier signals with adjacent center frequencies (closely spaced carriers). Because each generator is band limited, the conventional SISO DPD methods are not feasible and the MIMO DPD methods will not be suitable to represent nonlinear distortions because of the signal bandwidth expansion [23].

The work in [22] developed a multirate predistortion for a single transmission (SISO) that uses filtering to reduce the system analog bandwidth. In [22], the system (excitation and measurements) used smaller (analog) bandwidth and the predistortion computation enlarged the (digital) bandwidth to compute the basis through nonlinear operations and filtering. Note that, [22] resembles a similar approach to that presented in this paper although it is not suitable for multiple (multicarrier) transmissions. The ideas of [22] are extended in [23] to the case of dual-band concurrent transmitter. However, [23] considers the case of frequency-distant carriers, and hence, the predistortion ignores the effects of closely spaced carriers analyzed in this paper.

The nonlinear distortions under closely spaced concurrent carriers can be mitigated with the well-studied SISO DPD methods. These methods would form an aggregated digital domain using a single carrier [24], [26]. SISO DPD uses a single DAC stage with a high sample rate. This rate would be at least the sum of the individual rates required in each carrier. In concurrent systems with large bandwidth, such a high data rate increases the transmitter cost dramatically, which suggests that splitting the bandwidth before processing is more cost effective. Furthermore, splitting the bandwidth decomposes large dynamic effects making easier its compensation.

This paper describes a general class of nonlinear mitigation techniques that can be used for concurrent/aggregated carrier systems. We denote the proposed scheme the MIMO subband Volterra. In the method, the bandwidth is divided in subbands, and the processing of each subband includes linear and nonlinear effects. The technique is referred to as MIMO due to its architecture and it is applied to a concurrent carrier (multiband) scenario.

The proposed technique can be used with any MIMO model structure, like memory polynomials and sparse models. In particular, we used the MIMO Volterra series and explore three forms of pruned models. As with the SISO Volterra series, the MIMO subband Volterra is linear in the parameters and can be identified using robust and mature linear estimation techniques. This scheme is band limited similar to as [21]–[23]. However, it generalizes the approach by introducing the nonlinear distortion of different frequency bands in closely spaced carrier signals. The developed methodology can be used to design mitigation techniques both in satellite and terrestrial communications. The satellite scenario restricts

the uplink frequency band forcing the predistorted signal to be band limited, and the terrestrial one exhibits newer architectures [3] that support multiple carriers closely spaced in frequency. Discarding the effects of closely spaced carriers, in the proposed methodology, it renders models similar to those reported for typical concurrent terrestrial applications as in concurrent dual carrier [27], [28] and tricarrier [29], [30]. On the other hand, including these effects, it renders the model reported for multicarrier satellite scenarios [31]. Furthermore, the proposed technique can be used alternatively in traditional single transmission systems, in which the designer can split the overall bandwidth to reduce the costs and to make effective signal processing. A simulation of a subclass of the proposed DPD scheme is reported in [31], where the DPD is applied at the symbol level. In addition to [31], this paper evaluates the proposed DPD scheme in a realistic implementation using band-limited generators and a solid-state power amplifier. Furthermore, we analyze and discuss the HW impairments and the measurement challenges encountered at the transmitter deployment. This paper exemplifies the MIMO subband Volterra DPD technique by mitigating the nonlinear distortions in a triband concurrent aggregated system of large bandwidth (150 MHz of transmission bandwidth).

This paper is organized as follows. Section II describes the transmitter model architecture, presents its HW advantages and impairments, and makes a brief analysis of it using the MIMO Volterra theory. Section III describes the proposed DPD algorithm for such a transmitter analyzing its model complexity and devising suitable pruning techniques. The computational complexity is reviewed in Section IV, while the experimental setup and instrumentation challenges are presented in Section V. Section VI presents measurement results and comparisons of the proposed and previously published techniques. Finally, the discussions and the conclusions are drawn in Sections VII and VIII, respectively.

II. System Model

Consider K independent signals fed to a concurrent transmitter. Let $x_k(n)$ denote the kth complex-valued baseband sequence at the nth sampled instant. Each sequence is composed of the in-phase I_k and quadrature Q_k components $x_k(n) = I_k(n) + jQ_k(n)$. These sequences are converted into the analog, continuous time signals, $x_k(t)$ using DACs. In contrast to typical applications, where the sampling rate of the DAC (f_{DAC}) is set 4 to 8 times larger than the sample rate of the discrete signals, the architecture in Fig. 1 has DAC sample rates without oversampling. That is, f_{DAC} is equal to the sampling rate of the discrete signals, i.e., the DAC bandwidth is equal to the bandwidth of $x_k(t)$. These band-limited generators are unsuitable to deploy classical DPD methods, because they require more bandwidth for their excitation signals [22].

The signal $x_k(t)$ occupies a bandwidth of B_k Hz. The K signals are frequency multiplexed. That is, upconverted to a different carrier frequency f_k and combined. The center frequencies are equally spaced by Δf Hz. That is, $f_k = f_1 + (k-1)\Delta f$. This frequency planning favors distortion compensation, because distortions appear at the transmissions frequencies and hence its compensation becomes feasible [32]. The frequency-multiplexed bandpass signal is denoted by

$$u(t) = \sum_{k=1}^{K} \mathrm{Re}\{x_k(t) e^{j(2\pi f_k t + \varphi_k)}\} \tag{1}$$

where φ_k is the instantaneous phase of the kth local oscillator (LO) carrier frequency in the upconversion. The phases φ_k affect the baseband representation and they need to be considered for DPD.

The bandpass multicarrier signal $u(t)$ is forwarded through a power amplifier that produces nonlinear distortion. The output of the power amplifier $z(t)$ can be described by a Volterra series [33]. That is $z(t) = \mathbf{H}\{u(t)\}$, where $\mathbf{H}\{\cdot\}$ is an SISO Volterra operator. The output of the amplifier is filtered out before feedback measurements. This filter can be well represented by a finite impulse response (FIR) model in the baseband equivalent domain.

The filtered signal, $y(t)$, is measured in each frequency band rendering $y_k(n)$. The input/output relationships of $y_k(n)$ and $x_k(n)$ can be derived using the Volterra theory with a frequency-multiplexed input, similar to the derivations in [30]. For the sake of clarity, we point the result directly. The concurrent transmitter discrete baseband outputs $y_k(n)$ are described by an MIMO Volterra series [5] as

$$y_k(n) = y_k^{(1)}(n) + y_k^{(3)}(n) + \ldots y_k^{(p)}(n) \tag{2}$$

with the corresponding terms

$$\begin{aligned}
y_k^{(1)}(n) &= \sum_{k_1=1}^{K} \sum_{m_1=0}^{\infty} h_{k_1}^{(k)}(m_1) \tilde{x}_{k_1}(n-m_1) \\
y_k^{(3)}(n) &= \sum_{k_1,k_2,k_3=1}^{K} \sum_{m_1,m_2,m_3=0}^{\infty} h_{k_1,k_2,k_3}^{(k)}(m_1,m_2,m_3) \\
&\quad \times \tilde{x}_{k_1}(n-m_1) \tilde{x}_{k_2}(n-m_2) \tilde{x}_{k_3}^{*}(n-m_3) \\
&\vdots \\
y_k^{(p)}(n) &= \sum_{k_1,\ldots,k_p=1}^{K} \sum_{m_1,\ldots,m_p=0}^{\infty} h_{k_1,\ldots,k_p}^{(k)}(m_1,\ldots,m_p) \\
&\quad \times \prod_{i=1}^{\lceil p/2 \rceil} \tilde{x}_{k_i}(n-m_i) \prod_{j=1}^{\lceil (p-1)/2 \rceil} \tilde{x}_{k_j}^{*}(n-m_j)
\end{aligned} \tag{3}$$

where * denotes the conjugate operator, p represents the nonlinearity order of truncation, and $h_{k_1,\ldots,k_p}^{(k)}(m_1,\ldots,m_p)$ denotes the MIMO Volterra kernels for the kth output. $\tilde{x}_k$ is the baseband relative to the frequency-multiplexed signal of center frequency f_c, $\tilde{x}_k = x_k e^{j2\pi(f_k - f_c)t}$. Note that the notation for summations has been simplified. The indices in the sums represent independent summations. That is, $\sum_{m_1,m_2,m_3}^{\infty}$ is a short for $\sum_{m_1}^{\infty}\sum_{m_2}^{\infty}\sum_{m_3}^{\infty}$. These summations can be reduced, eliminating redundant terms, when considering the symmetry of MIMO Volterra series for real [34] or complex operators [1].

A block diagram of the considered system is shown in Fig. 1 for $K = 3$ carrier signals with an MIMO DPD scheme deployed using the indirect learning architecture [35].

Behavioral models of concurrent amplifiers have evolved toward the MIMO Volterra series. In dual-band concurrent systems, earlier models [13], [27] expand the series solely over its diagonal terms, similar to memory polynomials in SISO systems. Posterior dual models as [28] generalize the memory expansion as the MIMO Volterra. A similar trend is observed in triband concurrent systems from diagonal expansion of the series in [29] to an MIMO Volterra-like model in [30].

A. Hardware Impairments

1) IQ Imbalance: The IQ impaired complex-valued baseband signals (denoted by the underline) $\underline{x_k}(t)$ can be described by [36]

$$\underline{x_k}(t) = \alpha_k x_k(t) + \beta_k x_k^*(t) \tag{4}$$

where $\alpha_k = \cos(\theta_k/2) + j\gamma_k \sin(\theta_k/2)$, and $\beta_k = \gamma_k \cos(\theta_k/2) - j \sin(\theta_k/2)$ with real-valued γ_k and θ_k that denote the IQ gain and phase imbalance, respectively. No IQ imbalance is then $\alpha_k = 1$ and $\beta_k = 0$.

This model is extended to include the relative effects between different sources as

$$\underline{x_k}(t) = S_k\big(\alpha_k x_k(t) + \beta_k x_k^*(t)\big). \tag{5}$$

That is, the complex-valued factors S_k model the amplitude and phase difference of the IQ impaired basebands from different sources. Furthermore, without the loss of generality, we assume $S_1 = 1$, $S_k \neq 1$, and $\forall k \neq 1$. That is, the first carrier is chosen as reference.

Inserting the IQ impairments, (5), *into* (2) gives rise to new linear and nonlinear distortion products. In addition to (2), linear distortions of complex-conjugate inputs are produced. The factors S_k have a scaling effect on the linear and nonlinear distortions. Furthermore, the nonlinear distortions are dominated by $\underline{x_k}|\underline{x_i}|^2$, $\underline{x_i}^2\underline{x_k}^*$, and $\underline{x_i}\underline{x_k}\underline{x_\ell}^*$, where $\{k, i, \ell\}$ are the indices of the carriers. Expanding these IQ impaired nonlinear distortions, additional nonlinear distortions to the MIMO Volterra series are created, e.g., $x_k x_i^2$ and $x_k x_i^* x_i^*$. The reader is referred to Appendix A for the derivations. However, all the added nonlinear basis compared with (2) are scaled by a factor β_k/α_k, which is small number in realistic setups and applications [37]. Hence, the dominant nonlinear effects produced by the IQ impaired signal are included in (2).

2) Phase Noise: The kth LO introduces phase noise modeled by the random variable ϕ_k. This occurs at the up and downconversion. That is, the baseband carrier x_k transforms to $x_k e^{j\phi_k}$ [36]. The relative effects between different LO carriers are considered of two forms: noncoherent phase noises $\phi_1 \neq \phi_2 \neq \phi_3$ and coherent phase noise $\phi_1 = \phi_2 = \phi_3$. In a linear concurrent amplification, the distortions produced by the phase noise can be described by $x_k - x_k e^{j\phi_k}$. That is, phase noise affecting solely its carrier. However, for nonlinear (efficient) amplification, the phase noise of every oscillator contributes to the distortions in each carrier. See Appendix B for a brief discussion. Noncoherent LOs give an increased level of distortions compared with coherent LOs. The latter may, therefore, be used with simpler DPD algorithms.

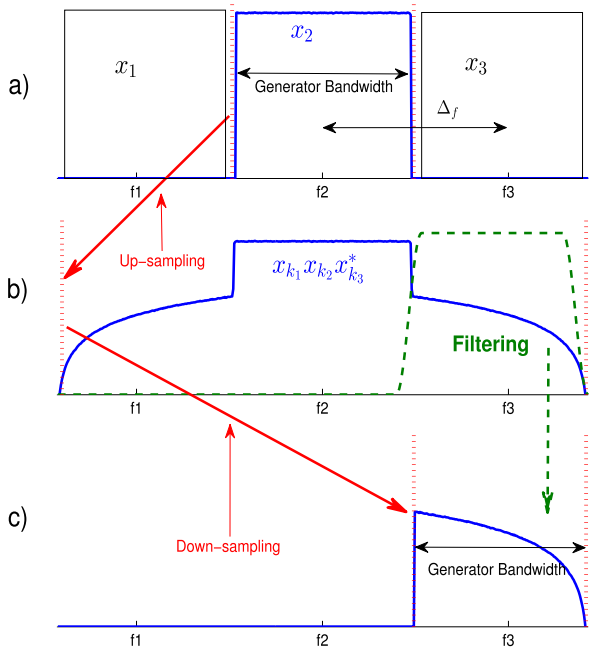

Fig. 2. Frequency domain illustration of the basis of the third-order nonlinear basis for the proposed DPD. (a) Carriers at the generators. (b) Upsampling, nonlinear operated and filtered to corresponding carrier. (c) Downsampling to the constrained generator bandwidth.

III. DPD Algorithm

A. MIMO Subband Volterra DPD

For the proposed DPD, the contribution of the basis functions in (2) is decomposed *into* different frequency bands. The third-order terms $x_{k_1}x_{k_2}x_{k_3}^*$ contribute to the frequency $f_{k_1} + f_{k_2} - f_{k_3}$ and exhibit a bandwidth of $\sum_{i=1}^{3} B_{k_i}$. The fifth-order terms $x_{k_1}x_{k_2}x_{k_3}x_{k_4}^*x_{k_5}^*$ contribute to the frequency $f_{k_1}+f_{k_2}+f_{k_3}-f_{k_4}-f_{k_5}$ with $\sum_{i=1}^{5} B_{k_i}$ bandwidth. For a pth order DPD, such bandwidth expansion needs to be considered if the carrier spacing Δf fulfills

$$\Delta f \leq p \ \max(B_1, B_2, \ldots, B_K) \tag{6}$$

where $\max(\cdot)$ is the maximum value operator.

The MIMO subband DPD scheme is based on multirate processing that enables the representation of nonlinear operators by band-limited predistorted signals at reduced rate for the generators (see Fig. 1). The band-limited baseband signals $x_k(n)$ are upsampled by a factor q. These upsampled sequences are forwarded through the MIMO Volterra model and then frequency shifted in order to correctly represent the sequences in the subband that should be mitigated. Finally, using an antialias (band limited) filter, the sample rate is reduced (downsampling by a factor q) to the DAC's rate. The frequency domain formulation of a nonlinear basis in the MIMO subband Volterra is shown in Fig. 2.

A block diagram of the proposed MIMO subband DPD for carrier 1 is shown in Fig. 3. This process mimics the signal flow in a concurrent carrier system, as shown in Fig. 1. So, the DPD scheme describes accurately the distortion effects at the output of the transmitter and consequently has excellent compensation ability for the considered frequency bands.

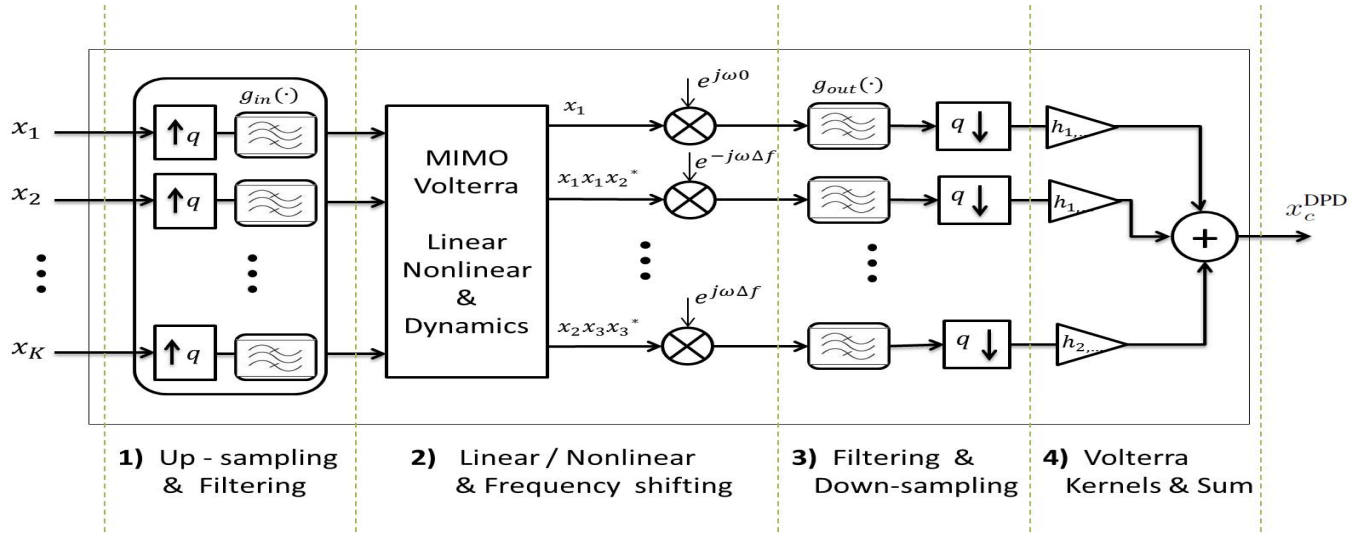

Fig. 3. DPD block diagram of the carrier 1 ($c = 1$) for concurrent aggregated carrier systems.

The MIMO subband DPD in Fig. 3 has the following stages.

1) *Input Upsampling and Filtering:* q upsampling increases the digital bandwidth of the signals by a factor q and the filtering process [with $g_{\mathrm{in}}(\cdot)$] mimics the generators linear effects due to the constraint bandwidth.
2) *MIMO Volterra and Frequency Shifting:* The upsampled and filtered signals from stage 1 propagate through an MIMO Volterra series. Due to enlarged digital bandwidth, nonlinear operators are faithfully described. According to the previous discussion, the output terms contribute to different frequency locations. So, using the LO carrier frequencies, these terms can be aligned (frequency shifted) with the cth carrier to be compensated.
3) *Output Filtering and Downsampling:* The distortions contributing to the cth carrier are isolated using an antialias filter [$g_{\mathrm{out}}(\cdot)$]. This filter can also model linear distortion at cth receiver. Finally, the distortions are downsampled by a factor q to have the same bandwidth as the input sequences.
4) *Kernel Linear Combination:* Each basis is multiplied by a complex-valued Volterra kernel.

Table I summarizes the generation of the MIMO subband predistorter basis. For the cth carrier signal, this predistorter is formalized by

$$\begin{aligned} x_c^{\mathrm{DPD}}(n) = & \sum_{m_1=0}^{M_1} b_1^{(c)}(m_1)\mathbf{D}\{\bar{x}_c(n'-m_1)\otimes g_{\mathrm{out}}(n')\} \\ & + \sum_{m_1=0}^{M_1} b_1^{\mathrm{IQ}(c)}(m_1)\mathbf{D}\{\bar{x}_c^*(n'-m_1)\otimes g_{\mathrm{out}}(n')\} \\ & + \sum_{k_1,k_2,k_3=1}^{K}\ \sum_{m_1,m_2,m_3=0}^{M_3} b_{k_1,k_2,k_3}^{(c)}(m_1,m_2,m_3) \\ & \mathbf{D}\{\bar{x}_{k_1}(n'-m_1)\bar{x}_{k_2}(n'-m_2)\bar{x}_{k_3}^*(n'-m_3) \\ & e^{j2\pi(f_{k_1}+f_{k_2}-f_{k_3}-f_c)n'}\otimes g_{\mathrm{out}}(n')\} + \\ & \vdots \end{aligned} \tag{7}$$

TABLE I
CONSTRUCTION OF BASIS IN THE SUBBAND DPD

Step	Procedure
1	Up-sample independently each baseband input signal.
2	Filter independently each upsampled signal (with $g_{in}(\cdot)$).
3	Create the MIMO Volterra basis (linear and nonlinear products).
4	Augment the linear basis with its complex-conjugate pairs to enhance the IQ impairment compensation.
5	Frequency shift the MIMO Volterra basis to its contribution bands.
6	Filter the shifted basis (with $g_{out}(\cdot)$) limiting its content to the compensation bandwidth.
7	Down-sample the filtered basis (with the same factor as step 1).

where $\bar{x}_k(n')$ denotes the kth upsampled and filtered [with $g_{\mathrm{in}}(\cdot)$] discrete sequence, $\otimes$ denotes the convolution operator, n' is used to denote the different sample rates, $\mathbf{D}\{\cdot\}$ denotes the downsampling operator $n' \rightarrow n$, and $b_{k_1,\ldots}^{(c)}$ denotes the complex-valued predistorter kernels. The second summation compensates for the linear IQ impairments, as discussed in Appendix A.

The filtering stages $g_{\mathrm{in}}(\cdot)$ and $g_{\mathrm{out}}(\cdot)$ (see Fig. 3) can be chosen independently of each other. This gives an extra degree of freedom to the DPD designer and the possibility to use some system knowledge to enhance the compensation abilities of the DPD scheme. Although in practice the generator and receiver responses [modeled by the filters $g_{\mathrm{in}}(\cdot)$ and $g_{\mathrm{out}}(\cdot)$] are generally unknown, experimental results using band-limiting functions of linear phase provide good results for this scheme. For carrier signals modulated with M-ary transmissions, both filters can be chosen to be the pulse shapers. In this way, the process emulates the transmitter and receiver structures resulting in a simple implementation and good performance results [31]. For a pth nonlinear order, MIMO subband DPD, the up and downsampling factor q is set as $q = \lceil p(\Delta f/\max(B_k))\rceil$ and can be adjusted for each

TABLE II

INDEX k_1, k_2, AND k_3 OF THE BASIS FUNCTIONS FOR THE THIRD-ORDER KERNEL $x_{k_1} x_{k_2} x^*_{k_3}$ IN THREE-CARRIER SYSTEM AT THE cth CARRIER. TOTAL # BASIS AND IN PARENTHESIS, SELF-MODULATION AND INTERMODULATION

$f_{k_1} + f_{k_2} - f_{k_3} - f_c$	$-\Delta f$	0	Δf	# basis
c = 1	-	111	121	10 (4)
	112	122	132	
	123	133	222	
	-	223	233	
c = 2	111	121	333	12 (4)
	122	132	322	
	133	222	311	
	223	233	221	
c = 3	121	333	-	10 (4)
	132	322	332	
	222	311	321	
	233	221	-	

TABLE III

INDEX k_1, k_2, k_3, k_4, AND k_5 OF THE BASIS FUNCTIONS FOR THE FIFTH-ORDER KERNELS $x_{k_1} x_{k_2} x_{k_3} x^*_{k_4} x^*_{k_5}$ IN A THREE-CARRIER SYSTEM AT cth CARRIER. $f_{\text{Dist}} = f_{k_1} + f_{k_2} + f_{k_3} - f_{k_4} - f_{k_5}$

$f_{Dist} - f_c$	$-2\Delta f$	$-\Delta f$	0	Δf	$2\Delta f$	# terms
c = 1	11113	11112	11111	11211	11311	42 (10)
	11122	11213	11212	11312	12211	
	11223	11222	11313	12212	12312	
	11333	11323	11322	12313	13313	
	12233	12223	12213	12322	13322	
	-	12333	12222	13323	22212	
	-	22233	12323	22213	22313	
	-	-	13333	22222	22322	
	-	-	22223	22323	23323	
	-	-	22333	23333	33333	
c = 2	11112	11111	11211	11311	12311	44 (10)
	11213	11212	11312	12211	13312	
	11222	11313	12212	12312	22211	
	11323	11322	12313	13313	22312	
	12223	12213	12322	13322	23313	
	12333	12222	13323	22212	23322	
	22233	12323	22213	22313	33323	
	-	13333	22222	22322	-	
	-	22223	22323	23323	-	
	-	22333	23333	33333	-	
c = 3	11111	11211	11311	12311	13311	42 (10)
	11212	11312	12211	13312	22311	
	11313	12212	12312	22211	23312	
	11322	12313	13313	22312	33313	
	12213	12322	13322	23313	33322	
	12222	13323	22212	23322	-	
	12323	22213	22313	33323	-	
	13333	22222	22322	-	-	
	22223	22323	23323	-	-	
	22333	23333	33333	-	-	

nonlinear order making efficient signal processing computations. For example, using $q = 4$ for the third-nonlinear order and $q = 6$ for the fifth-nonlinear order, respectively.

Table II indicates the basis functions for the nonlinear third-order kernel of the MIMO subband Volterra DPD in (7) at the cth carrier. Static third-order nonlinear distortion spans equally over adjacent carriers that make Table II cell symmetric (shown in gray shade). The columns in Table II indicate whether the basis is a self- modulation or intermodulation (column 0) or it is caused by adjacent distortion (columns $\pm\Delta f$). The last column in Table II indicates the number of contributing basis functions per carrier, in parenthesis, the number of contributing basis if carriers were large frequency spaced (self-modulation and intermodulation). In case of frequency-distant carriers, the column 0 contains the required basis for the DPD algorithm yielding similar models to those reported in the literature [29], [30].

Table III indicates the contributing basis functions for the fifth nonlinearity order kernel of the MIMO subband Volterra DPD for the cth carrier. Note that the number of contributing kernels increases fast with nonlinear order, which underlines the need for complexity reduction. In the following, we survey this problem in more detail.

B. Pruning

Table IV summarizes the number of contributing kernels in the MIMO subband Volterra scheme of nonlinearity order p with K aggregated carriers, in parenthesis, the number of coefficients in the kernel corresponding to self-modulation and intermodulation. By dividing the compensation bandwidth *into* smaller segments, the memory effects are effectively reduced per band. In this way, the memory depth required in the proposed technique is lower compared with an SISO model, which considers the whole bandwidth for processing. However, as it is pointed in Table IV, the number of coefficients in the kernels increases dramatically both with the number of carriers and with the nonlinear order. The number of kernels can be reduced with effective pruning methods. This has been an active area of research for SISO power amplifiers and it is now for multichannel systems. For instance, [12] proposes a pruning technique based on selecting the geometric paths of the MIMO Volterra series that covers the best its high dimensional space. On the other hand, [14] resources to sparse identification methods to select the MIMO Volterra basis that has the higher contribution to the output while discarding others. In the following, we describe novel ways of pruning the MIMO subband series that is suitable for concurrent amplification of closely spaced carriers.

1) Retaining Adjacent Distortions: Due to the bandwidth expansion of nonlinear operators, the higher the nonlinearity order the contributing terms span largely affecting other carriers. This is shown in Tables II and III, where the former has contribution from single adjacent distortion ($\pm\Delta f$), while the latter has contribution from two adjacent distortions ($\pm 2\Delta f$).

Due to the nonlinear distortion decay when shifting from its center frequency, a form of pruning can be made by discarding the terms from nonadjacent distortions. That is, removing all terms corresponding to columns $\pm 2\Delta f$ from Table III. Using this pruning technique, the number of contributing terms drops from 42 to 27 in the outer carrier and from 44 to 30 in the inner carrier. So, a total of 44 (out of 128) contributing terms of the fifth order are removed.

2) Diagonal MIMO Series: This pruning form is widely used in SISO [38] and in MIMO systems [27], [29]. It considers only equal memory depth in all basis functions in the MIMO series, e.g., using $m_1 = m_2 = m_3$ for the third-order terms in (7). This pruning significantly reduces the number of terms in the MIMO series. In the

TABLE IV

NUMBER OF STATIC CONTRIBUTING TERMS AT THE cth CARRIER IN THE pth NONLINEAR ORDER MIMO SUBBAND VOLTERRA WITH K AGGREGATED CARRIERS (IN PARENTHESIS, SELF-MODULATION OR INTERMODULATION, e.g., COLUMN 0 IN TABLES II AND III)

p	K	$c=1$	$c=2$	$c=3$	$c=4$	$c=5$	Total
3rd	2	5 (2)	5 (2)	-	-	-	10 (4)
	3	10 (4)	12 (4)	10 (4)	-	-	32 (12)
	4	17 (6)	20 (7)	20 (7)	17 (6)	-	74 (26)
	5	25 (9)	30 (10)	31 (11)	30 (10)	25 (9)	141 (49)
5th	2	11 (3)	11 (3)	-	-	-	22 (6)
	3	42 (10)	44 (10)	42 (10)	-	-	128 (30)
	4	109 (24)	119 (26)	119 (26)	109 (24)	-	456 (100)
	5	235 (50)	256 (54)	265 (57)	256 (54)	235 (50)	1247 (265)

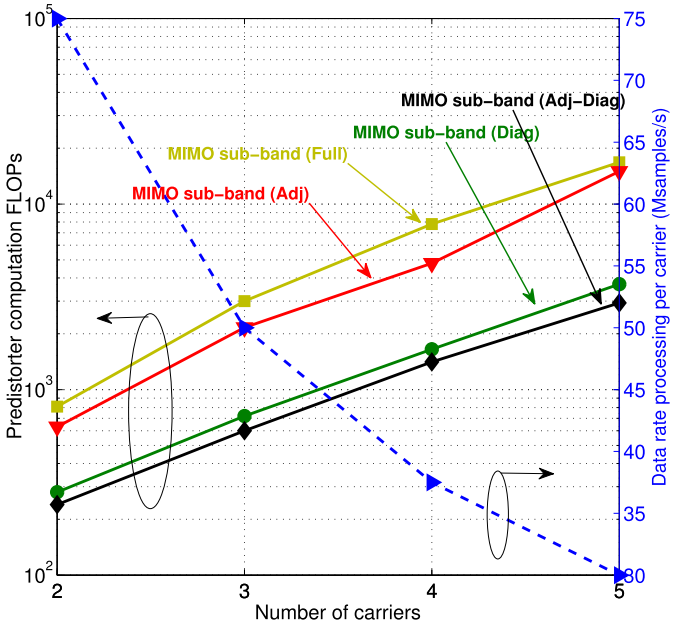

Fig. 4. Predistorter computation FLOPs and data rate processing versus the number of carrier signals.

considered scenario, using the third-order memory depth $M_3 = 1$ in the MIMO series gives 61 and 73 number of terms for the outer and inner carriers, respectively. On the other hand, using only the diagonal terms it reduces to 21 and 25 for the same carrier locations. So, a total of 128 (out of 195) contributing terms of the third order $M_3 = 1$ are removed.

The first pruning technique (retaining adjacent distortions) relies on the frequency representation of the MIMO Volterra basis selecting them accordingly to its band of influence. It is, therefore, different to other pruning methods as [12] and [14]. However, the second pruning technique (diagonal MIMO series) is a subset of [12] as it retains solely certain geometric paths in the MIMO Volterra series and discards the rest.

Table V lists the models tested in the experiments to validate the proposed methodology.

IV. COMPUTATIONAL COMPLEXITY

The digital computational complexity of the proposed technique was evaluated taking the methodology of [39]. The results are presented in Fig. 4, where the total number of floating point operations (FLOPs) in the predistorter computation

TABLE V

MIMO SUBBAND MODELS TESTED IN THE THREE CONCURRENT-AGGREGATED CARRIER SYSTEMS

Model	Description
Full	The model in (7) using a nonlinear order $p = 5$ and memory depths $M_1 = 7$ (linear), $M_3 = 1$ (third) and $M_5 = 0$ (fifth order).
Adj.	The full model in (7) pruned retaining only adjacent distortions.
Diag.	The full model in (7) pruned using $m_1 = m_2 = \ldots m_K$.
Adj-Diag.	The full model in (7) pruned combining the two previous pruning forms.

is seen as a function of the number of carriers (band segments) in the proposed subband DPD. Fig. 4 shows the computational complexity of the different models presented in Table V. Assuming a fixed transmission band (e.g., 150 MHz as used in this paper), Fig. 4 also plots the digital processing rate required per carrier. That is, the processing rate reduces proportionally with the number of subbands used. Fig. 4 shows the tradeoff encountered by using this technique. While increasing the number of carriers reduces the HW cost and digital processing rate, this increase also causes the growth of the MIMO Volterra series and the predistorter computation. The HW costs of each ADC/DAC stage and its power consumption are technology-dependent for the specific scenario and require a study before gains can be claimed. However, an example in [8] found cost savings of the order of 20 times in the ADC stage and power consumption reductions of seven times when using reduced bandwidths.

V. EXPERIMENT

A. DPD Instrumentation Challenges

A concurrent DPD requires control of the input excitation signals and a synchronized measurement of the output signals. We now describe the measurement challenges of a multiband DPD implementation using typical IQ RF front end for upconversion and downconversion (see Fig. 1).

1) Signal Generation: A baseband DPD requires that all discrete signals $x_k(n)$ are faithfully represented as they appear in the analog domain $x_k(t)$. This requires time synchronization between the independent basebands. That is, the digital to analog conversion of every carrier starts at the same *"reference"* time and preferably using the same DAC sampling rate. This is referred to as baseband coherency. This can be achieved

by triggering the baseband of the generators with a common signal and setting the same sampling clock for the DACs.

The RF upconversion in (1) alters the baseband signals by a phase shift (or phase rotation) with phase φ_k from the LO carrier phase. Furthermore, since nonlinear distortions are created as the products of the input baseband signals its compensation requires constant LO phases in the upconversion. This is a stringent requirement for the RF HW associated with the phase stability of the carrier oscillators. In a DPD implementation, the phases of the LO carriers have to remain stable between the initial measurements required to estimate the model and when deploying DPD. Our setup uses an instrument specifically designed to enhance phase stability of different LO frequencies [40].

2) Signal Measurement: Measurements are typically obtained through a downconversion process as

$$r(t) = G(y(t)e^{-j(2\pi f_c t+\psi)}) \tag{8}$$

where $y(t)$ denotes the passband frequency-multiplexed analog output of the concurrent transmitter that is downconverted to lower frequency, f_c denotes the LO demodulation carrier frequency, and ψ its instantaneous phase. $G(\cdot)$ is a linear filter modeling the receiver response.

A measurement of the multiple carriers can be performed in a single take when the receiver $G(\cdot)$ has sufficient bandwidth or in a sequential manner for a band limited receiver by sweeping f_c through f_k [32], [41]. The former requires larger analog bandwidth and faster ADC sampling rate and digital postprocessing to convert the signals into its baseband domain, whereas the latter works with repetitive signals and postprocessing using time delay estimation.

For adapting online DPDs, if several measurements are performed, the phase of the different LOs in the demodulator must be constant between each other similar to the requirement of the signal generation. In a lab setup and for calibration purposes, the frequency-multiplexed signal with extended bandwidth requirements can be measured with stitching techniques [42] and pilot injections [43].

B. Measurement Setup

The measurement setup is shown in Fig. 1 and it is composed of three Rohde & Schwarz SMBV100A vector signal generators. The three generators had a master/slave configuration and a trigger signal for the baseband synchronization. The DAC sampling rate of each generator was set to 50 MHz while the bandwidth of each excitation signal was 45 MHz. These three independent excitation signals were random-phase multisines with more than 5000 tones and a peak to average power ratio (PAPR) of approximately 9 dB. The frequency-multiplexed signal had a PAPR of around of 10.5 dB. The RF phase coherency of the three generators was enhanced using a Holzworth HS9003 coherent signal generator. This generator provides phase coherent multiple-RF outputs [40] used as LOs for up-conversion.

A 6-way splitter (Mini Circuits ZB6PD-2) with three 50 Ohm terminated paths was used to combine the excitation signals yielding a frequency-multiplexed signal of 150 MHz centered at 2.14 GHz. This frequency-multiplexed signal was

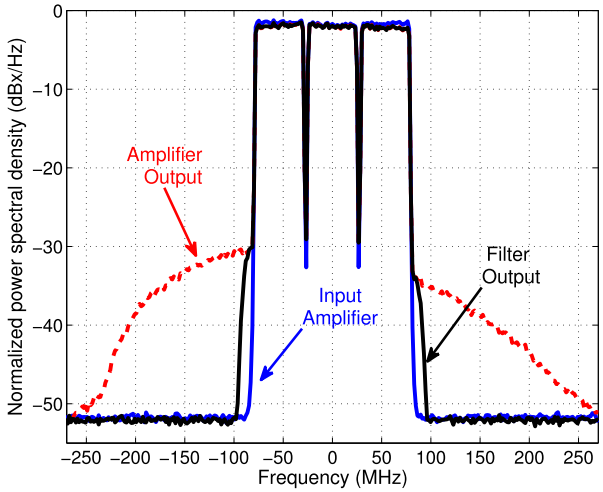

Fig. 5. Normalized power spectrum of the amplifier output and filter effect.

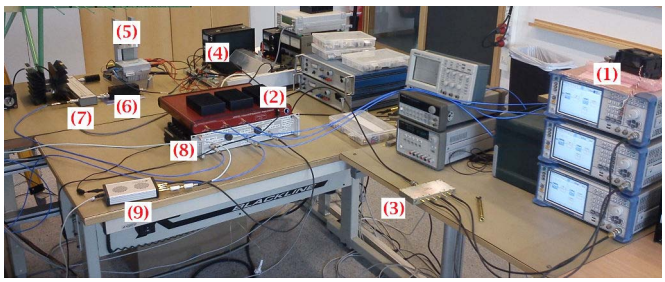

Fig. 6. Photograph of the experimental setup used to evaluate the feasibility of the proposed DPD. (1) Signal generators, (2) coherent generator, (3) combiner, (4) driver amplifier, (5) Doherty amplifier, (6) cavity filter, (7) directional coupler, (8) wideband down-converter, (9) ADC.

fed to a Freescale Semiconductor MRF8S21120HS Doherty amplifier through a linear driver amplifier. The out-of-band nonlinear distortions at the amplifier output were removed using a cavity filter. The passband of this filter is the same as the band used in the multiplexed signal. This is depicted in Fig. 5 where independent measurements with an spectrum analyzer (Rohde & Schwarz FSQ 26) were performed.

The feedback measurement loop (see Fig. 1) was assembled with a dual high-power directional coupler (Hewlett Packard 772D) at the transmitter output. The measurements were performed through a large bandwidth in-house down-converter connected to a high-performance SP devices ADC ADQ214 with 14-bit resolution operated at 400 MHz of sampling rate. A photograph of the experimental measurement setup is shown in Fig. 6.

The DPD was performed "off-line" using a PC to compute the predistorted sequences sent to the signal generators. 1×10^5 complex-valued baseband samples were measured per carrier and 30% of the samples were used to estimate the DPD while the rest was used for evaluation. The filtering stages in the proposed technique [$g_{\text{in}}(\cdot)$ and $g_{\text{out}}(\cdot)$] were chosen to be the same. These filters were modeled as an FIR with passband equal to the upsampled input signals using 52 real-valued coefficients. In the evaluation, only the steady state response of $g_{\text{in}}(\cdot)$ and $g_{\text{out}}(\cdot)$ was used, eliminating transients [22]. Hence, the linear phase of these filters will not affect the performance

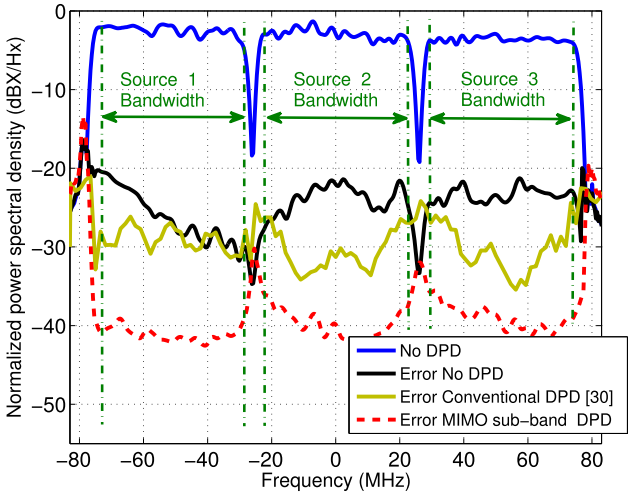

Fig. 7. Normalized power spectrum of the output signal with the 3-carriers and of the error spectrum with and without DPD. The MIMO sub-band DPD uses the "Full" model in Table V.

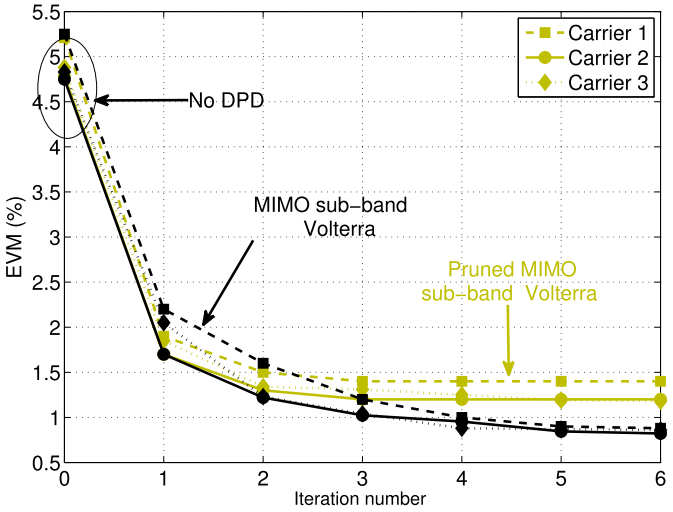

Fig. 8. EVM (in %) as a function of the number of DPD iterations. The Full MIMO Volterra (dark), the pruned (Adj-Diag. in Table V) Volterra (light).

of the method. The proposed DPD is tested using four different MIMO subband models described in Table V.

VI. Results

Fig. 7 shows the normalized error power spectral density of the measured frequency-multiplexed signals with and without DPD. Due to the narrow transition band in the cavity filter at the amplifier output (see Fig. 5), the uncompensated signal shows significant levels of error (distortions) with strong frequency-dependent effects. Despite that the concurrent DPD [29] was developed for frequency-distant carriers, it was implemented for benchmarking. [29] reduces the level of error (see Fig. 5). However, this method ignores the nonlinear effects of closely spaced carriers (due to its design) and would require larger generator bandwidth. Hence, [29] has limited mitigation abilities for the scenario described. Finally, the MIMO sub-band DPD method reduces significantly the level of error as observed in Fig. 7.

As the proposed DPD compensates for the in-band error it is suitable to evaluate its performance using the error vector magnitude (EVM). The EVM of the k-th carrier EVM_k is computed using N complex-valued samples as [44]

$$\mathrm{EVM}_k = \sqrt{\frac{\frac{1}{N}\sum_{n=1}^{N}|e_k(n)|^2}{P_{\mathrm{ref}_k}}}\ 100\% \qquad (9)$$

where $e_k(n)$ is the distortion at the k-th carrier defined as the difference between the input $x_k(n)$ and the scaled output of the transmitter $y_k(n)$. $P_{\mathrm{ref}_k} = 1/N\sum_{n=1}^{N}|x_k(n)|^2$ is the average power of $x_k(n)$.

Fig. 8 shows the EVM of the different carriers when the DPD is identified in an iterative off-line fashion. Iterative DPDs are performed according to [44] enhancing the performance by adapting to the device changes due to different signal excitations when estimating and deploying DPD models [45]. Because of the larger dimension of the models in the MIMO sub-band Volterra series they exhibit slower convergence than its pruned forms. However, these models can reach better EVM performances as observed in Fig. 8.

TABLE VI

EVM at the c-th Carrier With and Without DPD. The MIMO Sub-Band Uses Order $p = 5$ and Memory $M_1 = 7$, $M_3 = 1$, $M_5 = 0$ Pruned in Various Forms

DPD Scheme	# terms outer/inner	$c = 1$	$c = 2$	$c = 3$
No Mitigation	-	4.9%	4.7%	4.8%
Linear SISO per carrier	10×2 / 10	2.8%	2.4%	2.3%
MIMO sub-band (Full)	118×2 / 131	1.1%	1.0%	1.1%
MIMO sub-band (Adj)	103×2 / 117	1.2%	1.3%	1.3%
MIMO sub-band (Diag)	78×2 / 83	1.3%	1.2%	1.2%
MIMO sub-band (Adj-Diag)	63×2 / 69	1.3%	1.1%	1.2%

Table VI shows the EVM achieved in each carrier with and without DPD (after three iterations). A linear filter (FIR) with 10 complex-valued taps acting as DPD in each carrier is also included for comparison. This linear SISO DPD compensates linear dynamics revealing the level of uncompensated nonlinear effects. The proposed scheme captures these nonlinear effects offering enhanced EVM performance. Table VI reports the EVM for the 4 MIMO sub-band Volterra models indicated in Table V. That is, the full MIMO sub-band model and three pruned forms using adjacent terms (Adj.), diagonal memory (Diag.) and the combination of both pruning forms (Diag-Adj). As can be seen in Table VI all pruned forms of the MIMO sub-band DPD offer enhanced levels of EVM performance.

Fig. 9(a) presents the EVM as a function of the transmitter output power and power added efficiency. The uncompensated (No DPD) presents a deteriorated EVM that does not reduce at low power levels. The linear SISO DPD combats these effects offering improved performance at low output power levels. However, its EVM degrades rapidly for increasing power levels. The MIMO sub-band DPD offers enhanced EVM performance improving significantly the output power and the transmitter efficiency compared to the linear SISO DPD. The EVM of the MIMO sub-band DPD slightly degrades for higher power levels. This is a known effect caused by the increased PAPR in the predistorted signal [44]. Combining

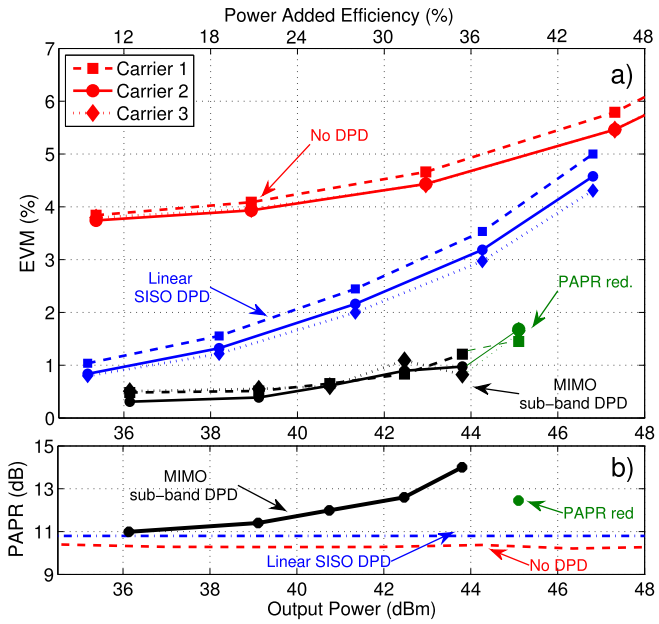

Fig. 9. EVM (in a) and PAPR (in b) as a function of the transmitter output power (in the lower x-axis) and efficiency (in the upper x-axis). The MIMO sub-band DPD uses the "Full" model in Table V.

a PAPR reduction technique for multiband transmitters [46] with the MIMO sub-band DPD, an increase in the output power can be obtained without sacrificing significantly EVM as observed in the most left points in Fig. 9(a). The PAPR of the frequency-multiplexed signal at the amplifier input is shown in Fig. 9(b). Both the No DPD and the linear SISO DPD have an unchanged level of PAPR with respect to the output power. On the other hand, the MIMO sub-band DPD increases PAPR with increasing output power. This increased PAPR exacerbates the amplifier compression effects and stress the need of PAPR reduction techniques in concurrent amplification.

VII. Discussion

The presented technique uses concurrent band-limited sources together with a digital mitigation technique to compensate nonlinear effects. The same technique can be applied (with the corresponding HW modifications) to a single-carrier ultra-wideband system by diving the excitation band. Similarly to single channel transmissions, this architecture presents HW impairments. Such impairments as IQ imbalance and phase noise may be tackled using digital compensations as briefly covered in this paper. The HW architecture requires baseband synchronization and the DPD performance benefits from RF phase coherency; DPD of concurrent dual-band transmitters for widely frequency-spaced signals would be affected in similar ways.

The proposed technique presents the tradeoff (a degree of freedom for designers) between computational complexity versus HW costs and data rate processing per carrier. As shown in Section IV the computational complexity increases with increasing number of carriers though the data rate per carrier decreases. It could make the technique less attractive for scenarios with many carriers (sub-bands). To mitigate this drawback, an approach similar to [32] could be used; i.e., performing a single DPD computation in the digital domain and relocate signal segments to different frequency bands (by several HW stages). This reduces the computational complexity but increases the digital rate processing of the predistorter (as typically encountered in SISO predistortion systems).

VIII. Conclusion

This paper presents a concurrent transmitter HW architecture with band-limited sources and an MIMO digital nonlinear mitigation technique designed for this HW scenario namely MIMO sub-band Volterra. The approach divides the band to be compensated considering linear and nonlinear effects from different carriers. The compensation in sub-bands combats effectively strong linear and nonlinear dynamic effects and allows reduced sample rate of the transmitter DAC stages. HW cost and power consumption are then reduced while keeping the EVM low. Hence it is a feasible architecture and DPD method for future wideband systems. The technique exploits digital multirate and filtering processes using the frequency planning of the carriers; thus, using system knowledge to enhance the performance of the compensation scheme. Furthermore, the technique can be used with any MIMO model structure, favoring those with easier estimation procedure (as linear estimation) and reduced computational complexity as pruned forms. Results in a 3-concurrent aggregated carrier transmitter using 50 MHz band-limited sources show an EVM below 1% for each carrier with significant gains in power efficiency and transmitted output power.

Appendix A
Concurrent IQ Impairments

Consider the k-th IQ-impaired baseband signal $\tilde{x}_k = \underline{x_k} e^{j\omega(f_k - f_c)t}$ with f_k as the carrier LO of and f_c as central carrier for baseband reference. The IQ impairment model is defined as $\underline{x_k} = S_k(\alpha_k x_k + \beta_k x_k^*)$. The linear distortions per carrier will follow the form $x_k(n) - \sum_{m=0}^{M} h_1^k(m)\underline{x_k}(n-m)$. Thus, in addition to the FIR filtered input, the distortion has a complex-conjugate pairs. This linear combination of complex conjugates are required in the DPD to provide the IQ impairment compensation ability [7], [45].

The largest nonlinear contributions can be analyzed by feeding the IQ-impaired frequency-multiplexed signal $x = \tilde{x}_1 + \tilde{x}_2 + \tilde{x}_3$ *into* a third-order static nonlinear model $y = x + h_3 x|x|^2$. The nonlinear distortions are produced by $h_3 x|x|^2$. According to the MIMO Volterra series in (2), these distortions can be grouped by its frequency contribution as $E_{f_k}^{\mathrm{IQ}} = h_3(I_{f_k} + A_{f_k})$ where $E_{f_k}^{\mathrm{IQ}}$ is the distortion centered at the f_k that can be regarded as in-band distortions I_{f_k} and injected adjacent distortions A_{f_k}

$$\begin{aligned} I_{f_1} &= \underline{x_1}|\underline{x_1}|^2 + 2\underline{x_1}|\underline{x_2}|^2 + \underline{x_2}^2\underline{x_3}^* + 2\underline{x_1}|\underline{x_3}|^2 \\ I_{f_2} &= 2\underline{x_2}|\underline{x_1}|^2 + \underline{x_2}|\underline{x_2}|^2 + 2\underline{x_1 x_3 x_2}^* + 2\underline{x_2}|\underline{x_3}|^2 \\ I_{f_3} &= 2\underline{x_3}|\underline{x_1}|^2 + 2\underline{x_3}|\underline{x_2}|^2 + \underline{x_2}^2\underline{x_1}^* + \underline{x_3}|\underline{x_3}|^2. \end{aligned} \quad (10)$$

Such distortions are caused by the IQ impaired inputs coupled with nonlinear effects. The terms A_{f_k} denote the adjacent

distortions injected to the f_k carrier. That is,

$$\begin{aligned} A_{f_1} &= I_{f_2} e^{j\omega\Delta_f t} + I_{o1} e^{-j\omega\Delta_f t} \\ A_{f_2} &= I_{f_1} e^{-j\omega\Delta_f t} + I_{f_3} e^{j\omega\Delta_f t} \\ A_{f_3} &= I_{f_2} e^{-j\omega\Delta_f t} + + I_{o3} e^{j\omega\Delta_f t} \end{aligned} \tag{11}$$

$I_{o1} = \underline{x_1 x_1 x_2}^* + \underline{x_1 x_2 x_3}^*$ and $I_{o3} = \underline{x_3 x_3 x_2}^* + \underline{x_3 x_2 x_1}^*$. The decomposition $E_{f_k}^{\mathrm{IQ}} = h_3(I_{f_k} + A_{f_k})$ it is the base of the sub-band approach and Table II shows its contributing terms. From (10) and (11), the nonlinear distortions are dominated by $\underline{x_k}|\underline{x_i}|^2$. Thus, inserting $\underline{x_k} = S_k(\alpha_k x_k + \beta_k x_k^*)$ *into* (10) and (11) this distortion can be decomposed. First notice

$$\begin{aligned} |\underline{x_i}|^2 &= |S_i|^2 |\alpha_i x_i + \beta_i x_i^*|^2 \\ &= |S_i|^2 \left[\alpha_i \beta_i^* x_i^2 + (|\alpha_i|^2| + |\beta_i|^2)|x_i|^2 + \beta_i \alpha_i^* x_i^* x_i^*\right] \\ &\approx |S_i|^2 \left[\alpha_i \beta_i^* x_i^2 + |\alpha_i|^2 |x_i|^2 + \beta_i \alpha_i^* x_i^* x_i^*\right] \end{aligned} \tag{12}$$

where the last approximation removes the term $|\beta_i|^2|x_i|^2$, because, ideally $\beta = 0$. Now, we form, $\underline{x_k}|\underline{x_i}|^2$ and remove the second and third-order products of β_k. That is, assume $\beta_k \beta_i = 0$. Then

$$\begin{aligned} \underline{x_k}|\underline{x_i}|^2 \approx S_k |S_i|^2 \big[&\alpha_i \alpha_k \beta_i^* x_k x_i^2 + \alpha_k |\alpha_i|^2 x_k |x_i|^2 \\ &+ \alpha_k \beta_i \alpha_i^* x_k x_i^* x_i^* + |\alpha_i|^2 \beta_k x_k^* |x_i|^2\big]. \end{aligned} \tag{13}$$

Factorizing $\alpha_k|\alpha_i|^2$ in (13) yields

$$\begin{aligned} \underline{x_k}|\underline{x_i}|^2 \approx \frac{S_k|S_i|^2}{\alpha_k|\alpha_i|^2} \Bigg[&\frac{\beta_i^*}{\alpha_i^*} x_k x_i^2 + x_k |x_i|^2 \\ &+ \frac{\beta_i}{\alpha_i} x_k x_i^* x_i^* + \frac{\beta_k}{\alpha_k} x_k^* |x_i|^2\Bigg] \end{aligned} \tag{14}$$

the relative amplitude of the distortions in (14) depend on the magnitude of the IQ imbalances, in particular of the ratio β_i/α_i. However, numerical evaluation of this ratio for realistic applications is lower than 1/15 [37]. This implies that the dominant distortion in (14) is $x_k|x_i|^2$.

Using the same simplifications

$$\begin{aligned} \underline{x_i}^2 \underline{x_k}^* &\approx \frac{S_i^2 S_k^*}{\alpha_i^2 \alpha_k^*} \left[x_i^2 x_k^* + 2\frac{\beta_i}{\alpha_i} x_k^* |x_i|^2 + \frac{\beta_k^*}{\alpha_k^*} x_i^2 x_k\right] \\ \underline{x_i x_k x_\ell}^* &\approx \frac{S_i S_k S_\ell^*}{\alpha_i \alpha_k \alpha_\ell^*} \Bigg[x_i x_k x_\ell^* + \frac{\beta_k}{\alpha_k} x_i x_\ell^* x_k^* \\ &\qquad + \frac{\beta_i}{\alpha_i} x_k x_\ell^* x_i^* + \frac{\beta_\ell^*}{\alpha_\ell^*} x_i x_k x_\ell\Bigg]. \end{aligned} \tag{15}$$

From (14) and (15), it can be seen that S_k have only scaling effects in the distortions. Furthermore, the dominant terms in the nonlinear IQ impaired distortions $\underline{x_i}^2 \underline{x_k}^*$ and $\underline{x_i x_k x_\ell}^*$ are $x_i^2 x_k^*$ and $x_i x_k x_\ell^*$, respectively. These distortion terms are covered by the MIMO sub-band DPD; therefore it offers IQ mitigation abilities for the dominant distortion effects produced by the IQ impaired inputs coupled to nonlinear effects. Since IQ impairments are systematic then, S_k, α_k and β_k are constant. By augmenting the model with the additional terms the IQ impairments can be compensated. However, to avoid large complexity, augmenting the model with the complex-conjugate pairs of the linear basis can be an alternative (as proposed in [45]).

APPENDIX B
PHASE NOISE

Consider the k-th phase noise impaired baseband signal $\hat{x}_k = x_k e^{j\phi_k} e^{j\omega(f_k - f_c)t}$ and the frequency-multiplexed $x = \hat{x}_1 + \hat{x}_2 + \hat{x}_3$. The phase noise in the k-th carrier is denoted by ϕ_k. In concurrent amplification the linear distortions are frequency-isolated and can be linearly approximated by $x_k - x_k e^{j\phi_k} \approx -j x_k \phi_k$, assuming ϕ_k relatively small. Thus, the linear distortions are proportional to the carrier and phase noise.

Propagating the frequency-multiplexed signal x through a nonlinear third-order model $h_3 x|x|^2$ the nonlinear in-band distortions per carrier can be frequency-isolated as

$$\begin{aligned} I_{f_1}^{\phi} &= h_3 \Gamma_1 x_1 e^{j\phi_1} + h_3 x_2^2 x_3^* e^{j(2\phi_2 - \phi_3)} \\ I_{f_2}^{\phi} &= h_3 \Gamma_2 x_2 e^{j\phi_2} + 2h_3 x_1 x_3 x_2^* e^{j(\phi_1 + \phi_3 - \phi_2)} \\ I_{f_3}^{\phi} &= h_3 \Gamma_3 x_3 e^{j\phi_3} + h_3 x_2^2 x_1^* e^{j(2\phi_2 - \phi_1)} \end{aligned} \tag{16}$$

where $I_{f_k}^{\phi}$ denotes the in-band distortions at the k-th carrier. Γ_k is an amplitude distortion function, $\Gamma_1 = |x_1|^2 + 2|x_2|^2 + 2|x_3|^3$, $\Gamma_2 = 2|x_1|^2 + |x_2|^2 + 2|x_3|^3$ and $\Gamma_3 = 2|x_1|^2 + 2|x_2|^2 + |x_3|^3$. The first terms in (16) show distortions of the phase noise per carrier while the second terms point out the phase noise distortions *injected* from the other carriers.

Two classes of LOs are considered: coherent and noncoherent. For noncoherent systems, the phases noises of different LOs are considered independent processes $\phi_1 \neq \phi_2 \neq \phi_3$, while for coherent systems [40], the phase noise is regarded as $\phi_1 = \phi_2 = \phi_3$ [47]. Taking the amplitude of $I_{f_1}^{\phi}$ distortion in (16) yields

$$\begin{aligned} \left|I_{f_1}^{\phi}\right|^2 = &\left|h_3 \Gamma_1 x_1\right|^2 + \left|h_3 x_2^2 x_3^*\right|^2 \\ &+ 2\Re\{|h_3|^2 \Gamma_1 x_1 \left(x_2^2\right)^* x_3 e^{j(\phi_1 + \phi_3 - 2\phi_2)}\} \end{aligned} \tag{17}$$

where $\Re\{\cdot\}$ returns the real part of its argument. The last term in (17) depicts the effects of phase noise, for coherent systems this term is invariant and deterministic while for noncoherent systems this term has increased variance. Thus, for noncoherent LOs the DPD identification degrades compared to coherent ones. For noncoherent LOs, lower phase noise gives better performance. Notice that the linearized system (when DPD is used) also can be described by a Volterra series. The h_3 term is then the residual third-order term that ideally should be zero. Using a linear approximation of the phase noise terms $e^{j\phi} \approx 1 + j\phi$, the residual distortion in (16) is then proportional to the phase noise for coherent LOs systems.

ACKNOWLEDGMENT

The authors would like to thank the anonymous reviewers for their valuable comments and suggestions to improve this manuscript.

REFERENCES

[1] S. Amin, P. N. Landin, P. Händel, and D. Rönnow, "Behavioral modeling and linearization of crosstalk and memory effects in RF MIMO transmitters," *IEEE Trans. Microw. Theory Techn.*, vol. 62, no. 4, pp. 810–823, Apr. 2014.

[2] Z. A. Khan, E. Zenteno, P. Händel, and M. Isaksson, "Digital predistortion for joint mitigation of I/Q imbalance and MIMO power amplifier distortion," *IEEE Trans. Microw. Theory Techn.*, Oct. 2016. [Online]. Available: http://ieeexplore.ieee.org/document/7600411/

[3] S. Bassam, W. Chen, M. Helaoui, and F. Ghannouchi, "Transmitter architecture for CA: Carrier aggregation in LTE-Advanced systems," *IEEE Microw. Mag.*, vol. 14, no. 5, pp. 78–86, Jul. 2013.

[4] T. Ali-Yahiya, *Understanding LTE and Its Performance*. New York, NY, USA: Springer, 2011.

[5] E. Zenteno, R. Piazza, M. R. B. Shankar, D. Rönnow, and B. Ottersten, "Low complexity predistortion and equalization in nonlinear multicarrier satellite communications," *EURASIP J. Adv. Signal Process.*, vol. 2015, no. 1, pp. 1–15, Mar. 2015.

[6] P. Singhal, P. Aggarwal, and V. Bohara, "Analysis of carrier aggregated OFDM signals in presence of dual band power amplifiers," in *Proc. 21st Nat. Conf. Commun. (NCC)*, Feb. 2015, pp. 1–6.

[7] Y.-J. Liu, W. Chen, J. Zhou, B.-H. Zhou, and Y.-N. Liu, "Joint predistortion of IQ impairments and PA nonlinearity in concurrent dual-band transmitters," in *Proc. 42nd Eur. Microw. Conf. (EuMC)*, Oct. 2012, pp. 132–135.

[8] Y. Liu, J. J. Yan, H. T. Dabag, and P. M. Asbeck, "Novel technique for wideband digital predistortion of power amplifiers with an undersampling ADC," *IEEE Trans. Microw. Theory Techn.*, vol. 62, no. 11, pp. 2604–2617, Nov. 2014.

[9] J. Kim, P. Roblin, D. Chaillot, and Z. Xie, "A generalized architecture for the frequency-selective digital predistortion linearization technique," *IEEE Trans. Microw. Theory Techn.*, vol. 61, no. 1, pp. 596–605, Jan. 2013.

[10] L. M. Li and S. A. Billings, "Generalized frequency response functions and output response synthesis for MIMO non-linear systems," *Int. J. Control*, vol. 79, no. 1, pp. 53–62, 2006.

[11] Z. K. Peng, Z. Q. Lang, and S. A. Billings, "Non-linear output frequency response functions for multi-input non-linear Volterra systems," *Int. J. Control*, vol. 80, no. 6, pp. 843–855, 2007.

[12] M. Younes and F. M. Ghannouchi, "Behavioral modeling of concurrent dual-band transmitters based on radially-pruned Volterra model," *IEEE Commun. Lett.*, vol. 19, no. 5, pp. 751–754, May 2015.

[13] S. A. Bassam, M. Helaoui, and F. M. Ghannouchi, "2-D digital predistortion (2-D-DPD) architecture for concurrent dual-band transmitters," *IEEE Trans. Microw. Theory Techn.*, vol. 59, no. 10, pp. 2547–2553, Oct. 2011.

[14] E. Zenteno, S. Amin, M. Isaksson, P. Händel, and D. Rönnow, "Combating the dimensionality of nonlinear MIMO amplifier predistortion by basis pursuit," in *Proc. 44th Eur. Microw. Conf. (EuMC)*, Oct. 2014, pp. 833–836.

[15] C. Quindroit, N. Naraharisetti, P. Roblin, S. Gheitanchi, V. Mauer, and M. Fitton, "FPGA implementation of orthogonal 2D digital predistortion system for concurrent dual-band power amplifiers based on time-division multiplexing," *IEEE Trans. Microw. Theory Techn.*, vol. 61, no. 12, pp. 4591–4599, Dec. 2013.

[16] Z. Huang, W. Chen, Z. Feng, and F. M. Ghannouchi, "Forward behavioral modeling of concurrent dual-band power amplifiers using extended real valued time delay neural networks," in *Proc. Int. Conf. Microw. Millim. Wave Technol. (ICMMT)*, vol. 5. May 2012, pp. 1–4.

[17] M. Younes and F. M. Ghannouchi, "On the modeling and linearization of a concurrent dual-band transmitter exhibiting nonlinear distortion and hardware impairments," *IEEE Trans. Circuits Syst. I, Reg. Papers*, vol. 60, no. 11, pp. 3055–3068, Nov. 2013.

[18] M. Cabarkapa, N. Neskovic, and D. Budimir, "A generalized 2-D linearity enhancement architecture for concurrent dual-band wireless transmitters," *IEEE Trans. Microw. Theory Techn.*, vol. 61, no. 12, pp. 4579–4590, Dec. 2013.

[19] M. Bozic and D. Budimir, "Joint compensation of I/Q impairments and power amplifier nonlinearity for concurrent dual-band transmitters using two-box model," *IEEE Microw. Wireless Compon. Lett.*, vol. 25, no. 5, pp. 340–342, May 2015.

[20] N. Naraharisetti, P. Roblin, C. Quindroit, and S. Gheitanchi, "Efficient least-squares 2-D-cubic spline for concurrent dual-band systems," *IEEE Trans. Microw. Theory Techn.*, vol. 63, no. 7, pp. 2199–2210, Jun. 2015.

[21] S. A. Bassam, A. Kwan, W. Chen, M. Helaoui, and F. M. Ghannouchi, "Subsampling feedback loop applicable to concurrent dual-band linearization architecture," *IEEE Trans. Microw. Theory Techn.*, vol. 60, no. 6, pp. 1990–1999, Jun. 2012.

[22] C. Yu, L. Guan, E. Zhu, and A. Zhu, "Band-limited Volterra series-based digital predistortion for wideband RF power amplifiers," *IEEE Trans. Microw. Theory Techn.*, vol. 60, no. 12, pp. 4198–4208, Dec. 2012.

[23] C. Yu, Y. Guo, and A. Zhu, "A band-limited 2-D digital predistorter for concurrent dual-band RF transmitters," in *Proc. IEEE Int. Wireless Symp. (IWS)*, Mar. 2014, pp. 1–4.

[24] N. Kelly, M. Allegue-Martínez, P.-D. Arapoglou, and A. Zhu, "Bandwidth-constrained digital pre-compensation technique for multi-carrier satellite communications," *Int. J. Satellite Commun. Netw.*, vol. 34, no. 2, pp. 171–194, 2016.

[25] R. H. Walden, "Analog-to-digital converter survey and analysis," *IEEE J. Sel. Areas Commun.*, vol. 17, no. 4, pp. 539–550, Apr. 1999.

[26] M. Isaksson, D. Wisell, and D. Rönnow, "A comparative analysis of behavioral models for RF power amplifiers," *IEEE Trans. Microw. Theory Techn.*, vol. 54, no. 1, pp. 348–359, Jan. 2006.

[27] S. A. Bassam, W. Chen, M. Helaoui, F. M. Ghannouchi, and Z. Feng, "Linearization of concurrent dual-band power amplifier based on 2D-DPD technique," *IEEE Microw. Wireless Compon. Lett.*, vol. 21, no. 12, pp. 685–687, Dec. 2011.

[28] J. Moon, P. Saad, J. Son, C. Fager, and B. Kim, "2-D enhanced Hammerstein behavior model for concurrent dual-band power amplifiers," in *Proc. 42nd Eur. Microw. Conf. (EuMC)*, Oct. 2012, pp. 1249–1252.

[29] M. Younes, A. Kwan, M. Rawat, and F. M. Ghannouchi, "Three-dimensional digital predistorter for concurrent tri-band power amplifier linearization," in *IEEE MTT-S Int. Microw. Symp. Dig.*, Jun. 2013, pp. 1–4.

[30] M. Younes, A. Kwan, M. Rawat, and F. M. Ghannouchi, "Linearization of concurrent tri-band transmitters using 3-D phase-aligned pruned Volterra model," *IEEE Trans. Microw. Theory Techn.*, vol. 61, no. 12, pp. 4569–4578, Dec. 2013.

[31] E. Zenteno, R. Piazza, M. R. B. Shankar, D. Rönnow, and B. Ottersten, "Multiple-input multiple-output symbol rate signal digital predistorter for non-linear multi-carrier satellite channels," *IET Commun.*, vol. 9, no. 16, pp. 2053–2059, 2015.

[32] C. Yu, J. Xia, X.-W. Zhu, and A. Zhu, "Single-model single-feedback digital predistortion for concurrent multi-band wireless transmitters," *IEEE Trans. Microw. Theory Techn.*, vol. 63, no. 7, pp. 2211–2224, Jul. 2015.

[33] M. Schetzen, *The Volterra and Wiener Theories of Nonlinear Systems*. New York, NY, USA: Wiley, 1980.

[34] A. K. Swain and S. A. Billings, "Generalized frequency response function matrix for MIMO non-linear systems," *Int. J. Control*, vol. 74, no. 8, pp. 829–844, Nov. 2001.

[35] C. Eun and E. J. Powers, "A new Volterra predistorter based on the indirect learning architecture," *IEEE Trans. Signal Process.*, vol. 45, no. 1, pp. 223–227, Jan. 1997.

[36] Q. Zou, A. Tarighat, and A. H. Sayed, "Joint compensation of IQ imbalance and phase noise in OFDM wireless systems," *IEEE Trans. Commun.*, vol. 57, no. 2, pp. 404–414, Feb. 2009.

[37] H. Cao, A. S. Tehrani, C. Fager, T. Eriksson, and H. Zirath, "I/Q imbalance compensation using a nonlinear modeling approach," *IEEE Trans. Microw. Theory Techn.*, vol. 57, no. 3, pp. 513–518, Mar. 2009.

[38] J. Kim and K. Konstantinou, "Digital predistortion of wideband signals based on power amplifier model with memory," *Electron. Lett.*, vol. 37, no. 23, pp. 1417–1418, Nov. 2001.

[39] A. S. Tehrani, H. Cao, S. Afsardoost, T. Eriksson, M. Isaksson, and C. Fager, "A comparative analysis of the complexity/accuracy tradeoff in power amplifier behavioral models," *IEEE Trans. Microw. Theory Techn.*, vol. 58, no. 6, pp. 1510–1520, Jun. 2010.

[40] H. Instrumentation, "Ultra low phase noise—Phase coherent synthesizers," *Microw. J.*, no. 10, pp. 48–50, Aug. 2009.

[41] C. Yu and A. Zhu, "Single feedback loop-based digital predistortion for linearizing concurrent multi-band transmitters," in *IEEE MTT-S Int. Microw. Symp. Dig.*, Jun. 2014, pp. 1–3.

[42] D. Wisell, D. Rönnow, and P. Händel, "A technique to extend the bandwidth of an RF power amplifier test bed," *IEEE Trans. Instrum. Meas.*, vol. 56, no. 4, pp. 1488–1494, Aug. 2007.

[43] E. Zenteno, M. Isaksson, and P. Händel, "Pilot tone aided measurements to extend the bandwidth of radio frequency applications," *Measurement*, vol. 90, pp. 534–541, May 2016.

[44] C. Nader, P. N. Landin, W. Van Moer, N. Bjorsell, and P. Händel, "Performance evaluation of peak-to-average power ratio reduction and digital pre-distortion for OFDM based systems," *IEEE Trans. Microw. Theory Techn.*, vol. 59, no. 12, pp. 3504–3511, Dec. 2011.

[45] L. Anttila, P. Handel, and M. Valkama, "Joint mitigation of power amplifier and I/Q modulator impairments in broadband direct-conversion transmitters," *IEEE Trans. Microw. Theory Techn.*, vol. 58, no. 4, pp. 730–739, Apr. 2010.

[46] B. Fehri, S. Boumaiza, and E. Sich, "Crest factor reduction of inter-band multi-standard carrier aggregated signals," *IEEE Trans. Microw. Theory Techn.*, vol. 62, no. 12, pp. 3286–3297, Dec. 2014.

[47] D. Rönnow, S. Amin, M. Alizadeh, and E. Zenteno, "Phase noise coherence of two continuous wave radio frequency signals of different frequency," *IET Sci., Meas. Technol.*, Sep. 2016. [Online]. Available: http://digital-library.theiet.org/content/journals/10.1049/iet-smt.2016.0203

Efrain Zenteno (S'10–M'16) received the B.S. degree from San Agustin University, Arequipa, Peru, in 2004, the M.Sc. degree in electronics/telecommunications engineering from the University of Gävle, Gävle, Sweden, in 2008, and the Ph.D. degree from the Royal Institute of Technology KTH, Stockholm, Sweden, in 2015.

He is currently with the Universidad Catolica San Pablo, Arequipa, where he is a Research Coordinator in science technology and innovation and has teaching duties with the Electronics and Telecommunication Department. His current research interests include instrumentation, measurements, and signal processing algorithms for communications.

Daniel Rönnow (M'05) received the M.Sc. degree in engineering physics and Ph.D. degree in solid-state physics from Uppsala University, Uppsala, Sweden, in 1991 and 1996, respectively.

From 1996 to 1998, he was with the Max-Planck-Institut für Festkörperforschung, Stuttgart, Germany, where he was involved in semiconductor physics. From 1998 to 2000, he was with Acreo AB, Stockholm, Sweden, where he was involved in infrared sensors and systems. From 2000 to 2004, he was a Technical Consultant and the Head of Research with Racomna AB, Uppsala, where he was involved in PA linearization and smart materials for microwave applications. From 2004 to 2006, he was a University Lecturer with the University of Gävle, Gävle, Sweden. From 2006 to 2011, he was a Senior Sensor Engineer with Westerngeco, Oslo, Norway, where he was involved with signal processing and seismic sensors. In 2011, he became a Professor of electronics with the University of Gävle. Since 2000, he has been an Associate Professor with Uppsala University. He has authored or co-authored over 45 peer-reviewed papers. He holds eight patents. His current research interests include RF measurement techniques and linearization of nonlinear RF circuits and systems.